Supplementary Information

for

"Near-Unity Unselective Absorption in Sparse InP Nanowire Arrays"

Katherine T. Fountaine,*[1,2,3] Wen-Hui Cheng,[2,3] Colton R. Bukowsky,[2] and Harry A. Atwater[2,3]

[1]NGNext, Northrop Grumman Aerospace Systems, 1 Space Park Dr., Redondo Beach, CA 90278

[2]Department of Applied Physics and Materials Science, California Institute of Technology, 1200 E. California Blvd., Pasadena, CA 91125

[3]Joint Center for Artificial Photosynthesis, California Institute of Technology, 1200 E. California Blvd., Pasadena, CA 91125

Supplementary Information

Absorption in the Cr and Ag

Figure 1 displays simulated absorption spectra for each material in the median tapered array. Note that a broadband source was used for this simulation, which requires a polynomial fit to the refractive index, as discussed in detail in the methods section. InP absorption beyond the band edge is a result of fitting errors.

Up to the band edge of InP (λ~925nm), the majority of the absorption occurs in the InP nanowires, and absorption contributions from the silver and chromium are negligible. Beyond the band edge, significant absorption occurs in the silver layer. At the silver interface, the nanowire radius is at a maximum, and because the radius was designed to achieve field enhancements up to the band edge, there are still significant field enhancements at slightly longer wavelengths, which, in the absence of InP absorption, enhances absorption in the silver in this region. Conversely, the Cr mask absorbs minimally because it is adjacent to regions of small nanowire radius, corresponding to field enhancements at shorter wavelengths where InP is strongly absorbing. In multi-radii arrays, both the Cr and the Ag absorb significantly beyond the band edge because the largest radius nanowire enhances the field near both the Cr and the Ag.

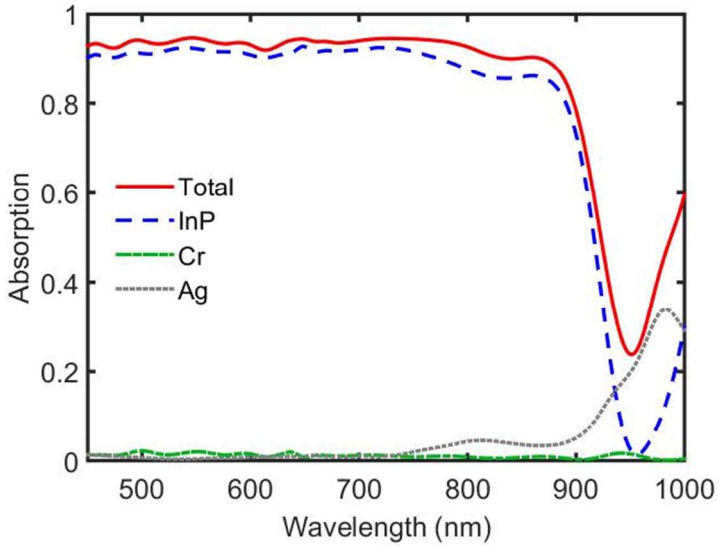

Figure 1: Simulated absorption vs. wavelength of the median tapered array with a back reflector, separated by material.

Sources of Deviation between Experimental and Simulated Spectra

The primary source for deviation between simulation and experiment arises from the approximate rendering of the nanowire shape. The top-down fabrication method results in a range of geometric shapes, primarily in the variation of the nanowire radius along its axis and the remains of the hard mask. Both the radial range and the profile shape varied between nanowires in a single array. All steps in the nanofabrication effect a certain degree of size variation, but the primary source is the high power, high temperature InP dry etch. Another large contribution comes from the peel-off step, in which the

fracture point of the wire varies and is challenging to quantify due to the difficulty of imaging of polymer-embedded nanowires. For the inverse taper, we assume the fracture point is the small point of the nanowire. This aspect adds uncertainty in the nanowire height, in addition to the radial profile. Accurate quantification of this great degree of geometric variation would require large scale three dimensional image analysis and accurate rendering would require insurmountable computation time. The simulated spectra, calculated from averages of multiple geometries, are therefore only approximate representations of the actual array, which accounts for deviations from the experimental spectra in the sharpness and prominence of small spectral features. That said, because the nanowires are only weakly interacting, the nanowire array design is robust and only requires a fairly even distribution of nanowire radii that have HE_{11} waveguide modes across the region of desired absorption enhancement. Furthermore, the weak inter-wire interaction implies that averaging simulated spectra of different nanowire array geometries is adequate for describing a single array with geometric variation.

For the results presented in Fig. 1 of the main text and Fig.2 of the Supplementary Information, another source of deviation between experimental and simulated spectra is the use of broadband FDTD simulations. We employed a commercial software package, Lumerical FDTD, that uses a polynomial fit to refractive index data across the simulated spectral range. In broadband simulations, these fits result in minor errors across the spectrum but are most pronounced near the band edge of InP at which the imaginary part of the refractive index fit does not equal zero. This fit error results in non-zero absorption beyond the band edge, which is unphysical. Broadband simulations were employed for these samples (Fig. 1 main text, Fig. 2 of SI) because they are more computationally efficient and the desired result was qualitative matching of the trends. For the near-unity absorbers in Fig.s 2 and 3 of the main text, single wavelength simulations were employed to eliminate this discrepancy source.

Reflectivity Spectra for Uniform Array

Figure 2 displays the simulated and experimental reflectivity spectra for the uniform array (SEM image shown in Fig. 1a of main text) in three different configurations—on substrate (red), on substrate and embedded in PDMS (yellow), and embedded in PDMS, peeled off from the substrate (green). These spectra illustrate good qualitative agreement between simulation and experiment (see above section for discrepancy sources) and also displays the low reflectivity of this array. Similar reflectivity spectra were observed for all samples discussed in this manuscript. The low reflectivity arises from the sparseness of the array and the efficient mode in-coupling, which is a product of the strong overlap of symmetry between the incident plane wave and the HE_{11} waveguide mode.

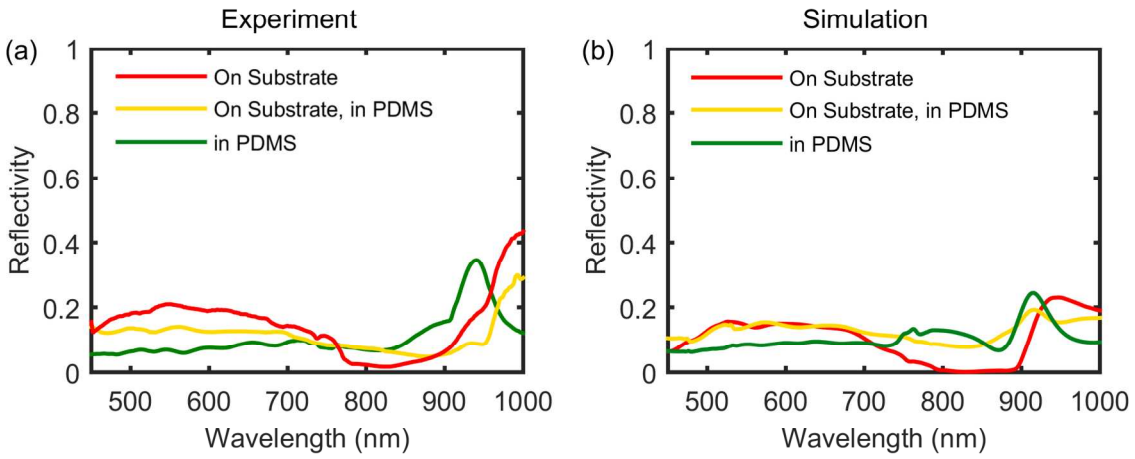

Figure 2: Reflection spectra of a uniform radius array. (a) Experimental and (b) simulated reflectivity spectra for the uniform radius array shown in Fig. 1(a) of the main text in three different configurations—on substrate (red), on substrate and embedded in PDMS (yellow), and the peeled array embedded in PDMS.

Simulated Dimensions

The top-down fabrication process resulted in significant geometric variation within a single array; therefore, in order to capture the optical behavior of the arrays, multiple array geometries were simulated.

For the arrays in Fig. 1 of the main text, broadband simulations were performed to cover the full range of geometries present in the arrays; the final simulated spectra are weighted averages of multiple geometries, with coefficients determined from a linear least squares fit to the experimental data. All combinations of the chosen parameter values were simulated. The parameters used for the simulation sweep of the uniform radius sample (Fig. 1a, main text) was top radius (82.5, 85, 87.5, 90 nm), normal radial taper (0, 5 nm), and wire height (1.5, 1.6 µm). The parameters used for the simulation sweep of the tapered sample (Fig. 1b, main text) was top radius (72.5, 75, 77.5, 80 nm), inverse radial taper (10, 15, 20 nm), and wire height (1.1, 1.2, 1.3 µm). The parameters used for the simulation sweep of the multi-radii sample (Fig. 1c, main text) was bottom radius of the smaller nanowire (30, 35, 40 nm), bottom radius of the larger nanowire (65, 70, 75), inverse radial taper (5, 10 nm), and wire height (1.3, 1.4 µm). The least squares fits resulted in down selection to two or three nanowire geometries; these geometries are summarized in Table 1.

Due to computational constraints for single wavelength simulations, simulation of the arrays in Fig. 2 and 3 of the main text were limited to three arrays with minor geometric variations; Fig. 2 used a standard mean of these three geometries and Fig. 3 used a weighted average determined from a linear least squares fit to the single pass, normal incidence experimental data (Fig. 3a of main text, red line). The three different geometries used for each array in the main text are summarized in Table 1.

Figure 3 displays the two geometries that were used to render the fabricated nanowires in simulation; the variable labels correspond to the labels and values presented in Table 1. Each row in the table is a separate simulation and braces are used to group wire sub-cells for the multi-radii arrays. The fill fractions, *ff*, and effective InP thicknesses, t_{eff}, are also calculated and included in the table, along with the coefficients, c_i, used for the weighted averages.

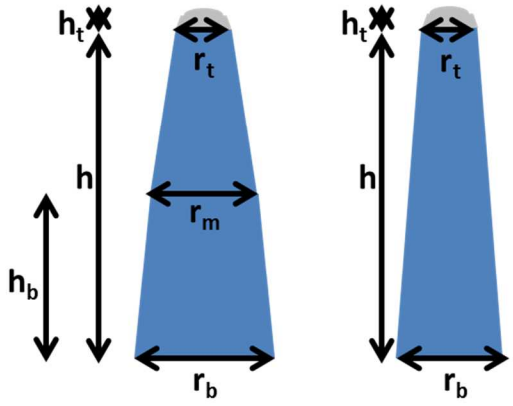

Figure 3: Schematic of two different nanowire geometries used in simulation; variables correspond to Table 1 values.

Table 1: Summary of array geometries used in simulation.

	[Fig1a]	[Fig1b]	[Fig1c]	[Fig2]	[Fig3]
r_b (nm)	87.5 90	62.5 57.5	{75,35} {75,35} {75,40}	100 107.5 112.5	{70,80,87.5,110} {70,82.5,92.5,115} {75, 82.5,97.5,115}
r_m (nm)	~	~	~	50 52.5 57.5	~
r_t (nm)	87.5 90	72.5 72.5	{85,45} {85,45} {85,50}	32.5 35 37.5	{35,42.5,55,67.5} {37.5,45,60,72.5} {42.5,50,62.5,75}
	1.6	1.3	1.4	1.55	1.7

h (um)	1.6	1.3	1.3 1.3	1.6 1.65	1.75 1.8
h_b (um)	~	~	~	0.775 0.8 0.825	~
h_t (um)	0.1	0.1	0.1	0.05	0.05
a (um)	0.75	0.75	0.75	0.45	0.52
c_i	0.64 0.36		0.37 0.56 0.07	.33 .33 .33	0.67 0.20 0.13
ff	0.043 0.045	0.024 0.022	0.022 0.022 0.030	0.057 0.067 0.078	0.058 0.064 0.068
t_{eff} (nm)	68 72	31 29	31 29 40	91 107 125	98 111 122